Proceedings of the 2007 IEEE/RSJ International
Conference on Intelligent Robots and Systems
San Diego, CA, USA, Oct 29 - Nov 2, 2007

Towards Batch Fabrication and Assembly of 3D Microstructures: A Sequential Assembly Planner with New Hard Magnet Configuration

Evan Shechter, Arjun Arumbakkam, Philip Lamoureux, Xueti Tang, Mutsuhiro Shima, Srinivas Akella
Rensselaer Polytechnic Institute

Abstract— **We propose a new method for assembly of 3D microstructures. Hard magnets are arranged in a novel 120° offset configuration, allowing for in-situ magnetization. The new configuration makes the use of hard magnets feasible in batch fabrication, and hard magnets allow for the use of a uniform external field for application of magnetic torque. A sequential planner was developed to calculate layout and magnet orientations for given assemblies, based on this new magnet configuration. We describe the new magnet configuration, experimentally test the configuration, and present a planner that generates a planar layout and magnet orientations.**

I. Introduction

3D microstructures have been used in devices such as microrobots [1],[3],[5], microsensors [6], and micro-optical devices [12]. As traditional micromachining is not well suited to fabricating complex 3D structures, self-assembly techniques assume significance. In this paper we introduce a self assembly method to build 3D microstructures from serially connected microfabricated panels.

We have developed a new magnet configuration and a corresponding assembly planner. In the new magnet configuration, all magnets on the die are oriented in one of three directions, equally separated by 120°. This directional classification of the magnets allows for batch deposition and magnetization of hard magnets, while retaining discrete control over torque direction of assembly in an external magnetic field.

The planner uses the magnet configuration to determine layout, magnet size, magnet orientation, and assembly sequence for a given 3D microstructure. The intent is that devices may be fabricated according to the planner output and will assemble and lock into the final configuration when placed in the correct magnetic field sequence. Towards this goal the contributions of this paper can be listed as follows:

- Hard magnet configuration for in-situ magnetization.
- Layout and Assembly planner, using the new magnet configuration.
- Experimental confirmation of new magnet configuration.

A. Assumptions

In this work, we assume that serial kinematic chains of hinged micropanels are fabricated with snap-fit locks that automatically engage when the micropanels are rotated to the specified dihedral angle (angle between adjacent micropanels). The dihedral angle is a function of the given 3D shape. We also impose the constraints that outermost panels fold first, and only static equilibrium conditions are considered when planning for the panel folding. These assumptions and constraints, together with the use of hard magnets and the novel magnet configuration allow for an algorithmic approach towards solving for a sequential assembly sequence of the microfabricated panel. Finally, in solving for the assembly sequence, the planner ignores stiction, electrostatic, van der waals forces, and hinge resistance. Techniques such as ultrasonic vibration during assembly have been shown to minimize these effects [2], [4]. In practice, we may also be able to compensate for any of these forces by increasing the net torque on each panel.

This work was supported in part by NSF under Award No. IIS-0093233 and Award No. IIS-0541224.

B. Organization

We describe the theory and justification for the new magnet configuration in Section II, present the layout and magnet planner algorithms in Section III, and show experimental results in Section IV. The experimental results demonstrate correct functionality of our magnet configuration, using macro-scale magnets.

II. Magnetic Actuation

The system we propose uses hard ferromagnets in a uniform external magnetic field for actuation. Hard and soft magnets differ in their hysteresis response, particularly in coercivity. The external field strength at which the magnetization goes to zero is called the coercive field strength, H_c, of the magnet. Hard magnets have greater coercive field strength than soft magnets.

When exposed to an external magnetic field, the domains of soft magnets will tend to realign so that the torque generated always moves the magnet in the direction of the negative gradient of the external field. The domains of hard magnets will not realign as readily due to their large coercive field strength, allowing us to assign the direction of torque by choosing the direction of domain alignment (magnetization).

Ferromagnets will experience torque when placed in uniform external magnetic fields. A magnet of volume V, with magnetic moment $\mathbf{M}$ in a uniform magnetic field $\mathbf{H}$, experiences a torque $\boldsymbol{\tau}$ given by [11]:

$$\boldsymbol{\tau} = V(\mathbf{M} \times \mathbf{H}) \tag{1}$$

There are cases in which non-trivial magnet arrangements must be used in order to correctly assemble the structure.

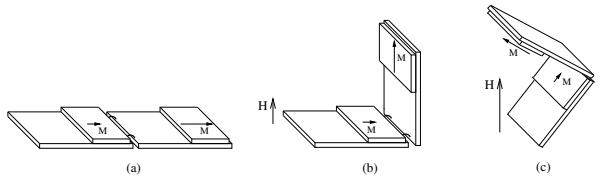

Fig. 1. Schematic diagram of two hinged panels. The magnetic moments of both magnets point in the same direction, but have different scalar moments (a). When exposed to small external magnetic field $\mathbf{H}$ the outer panel folds and locks in position (b). As $\mathbf{H}$ increases, both locked panels begin to rotate as a single unit and eventually reach equilibrium (c).

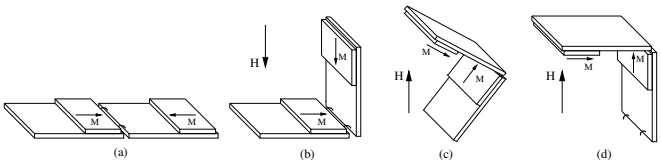

Fig. 2. Schematic diagram of two hinged panels. Magnets have opposite directions of magnetization (a). When exposed to external magnetic field $\mathbf{H}$, the outer panel folds and locks in position (b). After $\mathbf{H}$ reverses polarity, both locked panels begin to rotate as a single unit (c). Final configuration is reached and the lock engages before equilibrium. The locked configuration is shown (d).

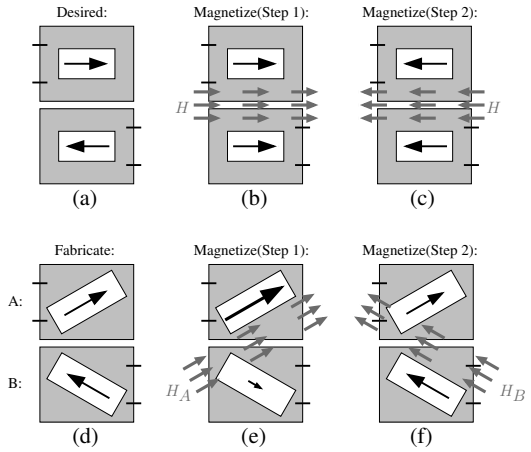

Fig. 3. Desired magnet configuration (a), setting magnetization direction of top magnet (b), setting magnetization direction of bottom magnet—note that top and bottom magnets are equally affected, making this configuration impossible to magnetize in-situ (c). In the proposed configuration, magnets are offset by 120°. The desired configuration is shown in (d). Note that the magnet magnitudes are slightly larger than in (a) to compensate for direction change. The top magnet is magnetized while the bottom magnet is only slightly affected (e). Finally the bottom magnet is magnetized, while the top magnet retains most of its original magnetization (f).

For example, the overhang structure shown in Figure 1 reaches magnetic torque equilibrium before assembling to the desired configuration. When a different set of magnets is used in which the magnets face opposite directions, and the external field alternates polarity, the structure fully assembles (Figure 2).

The high coercive field strength of hard magnets allows for in-situ magnetization in various directions, and therefore hard magnets can be used to control direction of torque during assembly. In the remainder of this paper we demonstrate our method of in-situ magnetization along various domain axes, and the algorithmic determination of magnet orientation and size, as well as device layout in order to successfully fabricate and assemble the structure.

A. New Magnet Configuration

Adhering magnets in the correct configuration on micro-scale devices is difficult, and not well suited to high volume fabrication. Our solution is to fabricate hard magnets in a set of three orientations, by taking advantage of shape anisotropy and coercivity of the magnets. In this case, we electroplate cobalt platinum (CoPt) on the devices.

Shape anisotropy is the tendency of the magnetic hysteresis to vary as the direction of external field moves from the long geometric axis to short, and vice versa. In general, rectangular magnets have lower demagnetizing fields along their long axes than along their short axes [8] This makes them easier to magnetize along their long axes, which are consequently called *easy axes.*

The CoPt film as deposited must be magnetized by exposure to a magnetizing field before it can be used to generate torque. The direction of magnetization is decided by the planner such that the resultant torque in an external magnetic field assembles the micropanel into its required configuration.

Two identical magnets on a single device will be magnetized in the same direction when exposed to a magnetizing field. Reversing direction of the field would reverse the magnetization of both magnets equally, as shown in Figure 3 a-c. This presents a problem when assembly requires torque in different directions.

Our solution to this problem is to take advantage of shape anisotropy by orienting the long axes of the magnet samples 120° apart from each other and magnetizing them along their long axes (Figure 3 d-f). The process can be explained as follows: Let magnet A be magnetized first by applying a magnetizing field $\mathbf{H}^\alpha$ along its long axis in the required $\mathbf{M}$ direction. This is followed by applying a magnetizing field $\mathbf{H}^\beta$ in the required $\mathbf{M}$ direction for a second magnet B. For magnet A to retain any magnetization in its intended direction, the component of $\mathbf{H}^\beta$ in the opposite direction of magnet A's magnetization must be less than the coercive field $\mathbf{H}_\mathbf{c}^\alpha$ of the magnet. When $\mathbf{H}^\beta$ is offset from $\mathbf{H}^\alpha$ by 120°, as in our system, the following constraint applies to the magnitude of $\mathbf{H}^\beta$:

$$|\mathbf{H}^\beta| < \frac{|\mathbf{H}_\mathbf{c}^\alpha|}{\cos 60^\circ} \tag{2}$$

Following this constraint, we can fabricate magnets in three directions, and magnetize them all in-situ, while retaining significant magnetization of each. The magnetic planner determines which direction should be chosen for each face.

III. ASSEMBLY PLANNING

In complex devices, the task of manually determining a layout and assembly sequence may be difficult to impossible. Lu and Akella [7] used motion planning algorithms for carton

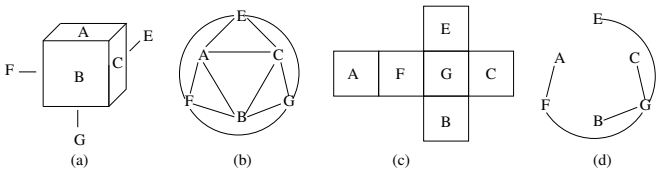

Fig. 4. A (a) cube with its (b) face connectivity graph, and a (c) planar net of the cube, with the (d) net's face connectivity graph.

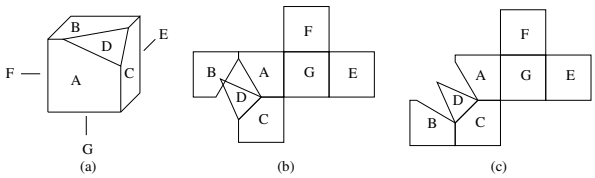

Fig. 5. A polyhedron (a), a representative net with internal intersections (b), and a representative net without intersections (c)

folding. We use a similar philosophy in using an assembly planning algorithm to enable the design of complex 3D microstructures. Given a representative planar net (flattened representation) and dihedral angles (angle between planes of two faces) for shared edges of the net, the assembly planner will determine position, orientation, and size of magnets that will result in correct assembly.

We assume that the external magnetic field $\mathbf{H}$ is always perpendicular to the substrate, and that the planner is given a scalar value of $\mathbf{H}$ as an input. The number of polarity changes required for complete assembly is output by the planner, along with the device and magnet layouts.

A. Layout Planner

The layout planner uses a face connectivity graph to represent both the input polyhedron and output layout. Each node of the graph represents a face of the polyhedron, and each edge of the graph represents adjacency of faces. Figure 4 illustrates the planar net and face connectivity representations of a cube.

We use the heuristic that it is best to minimize the longest sequential chain in any assembly. A corresponding net can be found by running a breadth-first search on the face connectivity graph, with the root of the search being the base of the assembly, and marking each node as it is visited so loops may be avoided. Breadth first search gives a minimum number of folds.

We must also ensure that the layout can be fabricated, and specifically, is not self-intersecting. An example of a convex polyhedron with a self-intersecting net is shown in Figure 5. It is conjectured that all convex polyhedra can be unfolded to a net that is not self-intersecting, but is still an open problem [9],[10]. By extension of the fact that the problem is still open, there are no known guaranteed algorithms for finding such a net other than brute force enumeration, if face cuts are not permitted.

During breadth-first unfolding, ties in depth are broken arbitrarily. These ties may arise due to the fact that there is no implicit order of node visitation within a given depth of the search. Self-intersection checking on the net is then performed. If there are any intersections in the net, we backtrack and repeat on all trees in different order of tie-breaking until a non-intersecting net is found.

B. Magnetics Planner

The magnetic planner finds magnet size and orientation, as well as external field direction, such that the device will correctly assemble. The magnets must have a long aspect ratio, as described in Section II-A. Hard magnets in a uniform external field generate pure torque, so position on the panel does not affect torque on the panel by the magnet. However, gravitational torque will be affected, so to simplify the planner we add the constraint that the center of mass of each of the magnets coincides with the center of mass of its respective face.

We use the term *tree* to describe a kinematic chain of faces (panels), derived from given net. Faces are denoted f, and a *root* face is the root of a given tree. In terms of the device, the root will be fixed to the substrate. A *subtree* of face f is a tree that is kinematically linked to f, and is farther from the base of the structure than f.

The planner recursively computes magnet size and orientation, as well as external field direction. It first determines the torque required to actuate the outermost panel (leaf) of each of the subtrees. Then it assigns a direction for the external magnetic field and determines direction and size of the magnet to be fabricated on that panel, taking into account the subtree attached to the panel, as well as the panel itself.

The planner then evaluates the face one level up from the leaf to determine magnet parameters. It calculates the magnet parameters based on the assumption that the subtree has now assembled into its folded and locked configuration, and is a single rigid body.

The calculation of magnetics parameters is described in detail below.

1) Magnet Mass Calculation: The magnetic torque $\boldsymbol{\tau^m}$ required to rotate a tree (at this point, a rigid body consisting of a chain of folded, locked panels) is set equal to the equilibrium torque $\boldsymbol{\tau^g}$ necessary to oppose gravity, multiplied by a user specified constant ϵ where $\epsilon \in \Re$, $\epsilon > 1$.

In the following equations, the variable m represents mass, $\boldsymbol{\mu}$ is magnetic moment, $\mathbf{M}$ is magnetic moment per unit volume, $\mathbf{g}$ is gravity, and $\mathbf{H_i}$ is an external magnetic field at step i.

We use the convention that a variable with the superscript ^{m} is related to magnetics. For example, $\boldsymbol{\tau^m}$ is magnetic torque, and m^m is mass of a magnet. The superscript ^{g} refers to gravity, so $\boldsymbol{\tau^g}$ is gravitational torque. Finally, the superscript ^{p} refers to panel. For example, the variable m^p represents the mass of a panel. In addition, subscripts are used to specify root $_r$, or subtree $_s$.

Magnetic moment $\boldsymbol{\mu}$ is related to volume independent $\mathbf{M}$:

$$\boldsymbol{\mu} = \mathbf{M}V = \frac{\mathbf{M}m}{d} \tag{3}$$

for a magnet of volume V, mass m, and density d.

Again, in the following equations, $\boldsymbol{\tau}$ represents torque, $\mathbf{r_r}$ is the distance vector from hinge axis to center of mass of the root panel, $\mathbf{r_s}$ is the distance vector from the root hinge axis to the center of mass of the subtree, m_r^m and m_s^m are mass of the root magnet and subtree magnets respectively, m_r^p and m_s^p are mass of the root panel and subtree panels respectively, $\mathbf{g}$ is gravity, and $\boldsymbol{\mu}$ is magnetic moment. A unit vector parallel to the hinge axis is denoted $\hat{e}$. We also have the reaction torque τ_R, which the hinge imposes to constrain motion along one axis.

The equations for gravitational torque $\boldsymbol{\tau^g}$ and magnetic torque $\boldsymbol{\tau^m}$ vectors are:

$$\begin{aligned}
\boldsymbol{\tau_r^m} &= \boldsymbol{\mu_r} \times \mathbf{H_i} = \frac{m_r^m}{d}\mathbf{M_r} \times \mathbf{H_i} && (4)\\
\boldsymbol{\tau_s^m} &= \boldsymbol{\mu_s} \times \mathbf{H_i} && (5)\\
\boldsymbol{\tau_r^g} &= \mathbf{r_r} \times (m_r^m + m_r^p)\mathbf{g} && (6)\\
\boldsymbol{\tau_s^g} &= \mathbf{r_s} \times (m_s^m + m_s^p)\mathbf{g} && (7)\\
\boldsymbol{\tau_R} &= \boldsymbol{\tau_r} + \boldsymbol{\tau_s} - [\hat{e} \cdot (\boldsymbol{\tau_r} + \boldsymbol{\tau_s})]\hat{e} && (8)
\end{aligned}$$

The mass of the magnet is also implicit in $\boldsymbol{\mu}$, so we need to further isolate these terms. The magnetic moment per unit volume is a material property, and is denoted $\mathbf{M}$. It follows that $\boldsymbol{\mu} = V\mathbf{M}$ and $\boldsymbol{\mu} = \frac{m}{d}\mathbf{M}$ for density d.

Setting $\boldsymbol{\tau^m}$ and $\boldsymbol{\tau^g}$ equal to each other multiplied by ϵ, we can then solve for the mass of the magnet on the root panel, m_r^m:

$$\begin{aligned}
\boldsymbol{\tau_r^m} + \boldsymbol{\tau_s^m} - \epsilon(\boldsymbol{\tau_r^g} + \boldsymbol{\tau_s^g}) + \boldsymbol{\tau_R} &= \mathbf{0} && (9)\\
\boldsymbol{\tau_r^m} - \epsilon\boldsymbol{\tau_r^g} + \boldsymbol{\tau_R} &= \epsilon\boldsymbol{\tau_s^g} - \boldsymbol{\tau_s^m} && (10)
\end{aligned}$$

$$\begin{aligned}
m_r^m \left(\frac{1}{d}\mathbf{M_r} \times \mathbf{H_i} - \epsilon\mathbf{r_r} \times \mathbf{g}\right) + \boldsymbol{\tau_R}\\
= \epsilon\boldsymbol{\tau_s^g} - \boldsymbol{\tau_s^m} + \epsilon m_r^p \mathbf{r_r} \times \mathbf{g} \quad (11)
\end{aligned}$$

The center of mass $\mathbf{r}$ of each panel is given as system specification. Due to the constraint that outermost panels fold first, we know that all children of any given panel are folded and locked before the panel itself will fold. This subtree of panels now forms a single rigid body, so we can calculate the new center of mass as the vector sum of the subtree center of mass and the parent panel's center of mass, which has been rotated to the hinge's dihedral angle:

$$\mathbf{r_r} = \frac{m_r^p \mathbf{r_r^p} + m_r^m \mathbf{r_r^m} + m_s \mathbf{r_s}}{m_r^p + m_r^m + m_s} \quad (12)$$

(11) becomes

$$\begin{aligned}
m_r^m \left(\frac{1}{d}\mathbf{M_r} \times \mathbf{H_i} - \epsilon\frac{m_r^p \mathbf{r_r^p} + m_r^m \mathbf{r_r^m} + m_s \mathbf{r_s}}{m_r^p + m_r^m + m_s} \times \mathbf{g}\right) + \boldsymbol{\tau_R}\\
= \epsilon\boldsymbol{\tau_s^g} - \boldsymbol{\tau_s^m} + \epsilon m_r^p \frac{m_r^p \mathbf{r_r^p} + m_r^m \mathbf{r_r^m} + m_s \mathbf{r_s}}{m_r^p + m_r^m + m_s} \times \mathbf{g} \quad (13)
\end{aligned}$$

To simplify the written form,

$$\begin{aligned}
&\text{let} \quad a = m_r^p + m_s\\
&\text{let} \quad \mathbf{q} = m_r^p \mathbf{r_r^p} + m_s \mathbf{r_s}\\
&\text{let} \quad \mathbf{s} = \frac{1}{d}\mathbf{M_r} \times \mathbf{H_i}\\
&\text{let} \quad \mathbf{t} = \epsilon\boldsymbol{\tau_s^g} - \boldsymbol{\tau_s^m}
\end{aligned}$$

$$\begin{aligned}
m_r^m \left(\mathbf{s} - \epsilon\frac{\mathbf{q} + m_r^m \mathbf{r_r^m}}{a + m_r^m} \times \mathbf{g}\right) + \boldsymbol{\tau_R}\\
= \mathbf{t} + \epsilon m_r^p \frac{\mathbf{q} + m_r^m \mathbf{r_r^m}}{a + m_r^m} \times \mathbf{g} \quad (14)
\end{aligned}$$

$$\begin{aligned}
m_r^m \left((a + m_r^m)\mathbf{s} - \epsilon(\mathbf{q} + m_r^m \mathbf{r_r^m}) \times \mathbf{g}\right) + \boldsymbol{\tau_R}\\
= (a + m_r^m)\mathbf{t} + \epsilon m_r^p (\mathbf{q} + m_r^m \mathbf{r_r^m}) \times \mathbf{g} \quad (15)
\end{aligned}$$

$$\begin{aligned}
m_r^m((a+m_r^m)\mathbf{s}+\epsilon(\mathbf{q}+m_r^m \mathbf{r_r^m})\times\mathbf{g}-\mathbf{t}-\epsilon m_r^p \mathbf{r_r^m}\times\mathbf{g})+\boldsymbol{\tau_R}\\
= a\mathbf{t} + \epsilon m_r^p \mathbf{q} \times \mathbf{g} \quad (16)
\end{aligned}$$

$$\begin{aligned}
m_r^m[m_r^m(\mathbf{s} - \epsilon\mathbf{r_r^m} \times g) + a\mathbf{s} - \mathbf{t}\\
- \epsilon(\mathbf{q} + m_r^p \mathbf{r_r^m}) \times \mathbf{g}] + \boldsymbol{\tau_R}\\
= a\mathbf{t} + \epsilon m_r^p \mathbf{q} \times \mathbf{g} \quad (17)
\end{aligned}$$

assigning more variables:

$$\begin{aligned}
&\text{let} \quad \mathbf{u} = \mathbf{s} - \epsilon\mathbf{r_r^m} \times \mathbf{g}\\
&\text{let} \quad \mathbf{v} = a\mathbf{s} - \mathbf{t} - \epsilon(\mathbf{q} + m_r^p \mathbf{r_r^m}) \times \mathbf{g}\\
&\text{let} \quad \mathbf{w} = a\mathbf{t} + \epsilon m_r^p \mathbf{q} \times \mathbf{g}
\end{aligned}$$

(17) becomes

$$(m_r^m)^2\mathbf{u} + m_r^m\mathbf{v} - \mathbf{w} + \boldsymbol{\tau_R} = 0 \quad (18)$$

We project vectors $\mathbf{u}$, $\mathbf{v}$, $\mathbf{w}$ onto the hinge axis before solving for m_r^m in (17). The reaction torque $\boldsymbol{\tau_R}$ then goes to zero. For a unit vector $\hat{e}$ parallel to the hinge axis,
$u = \mathbf{u} \cdot \hat{e}$, $v = \mathbf{v} \cdot \hat{e}$, $w = \mathbf{w} \cdot \hat{e}$
using the quadratic formula on u, v, w, we solve for m_r^m:

$$m_r^m = \frac{-v \pm \sqrt{v^2 + 4uw}}{2u} \quad (19)$$

Since mass m_r^m must be a real, non-negative number, we discard complex and negative roots from (19). The planner aborts if there are no real, non-negative solutions.

The mass given by (19) monotonically varies as a function of the dihedral angle of the root panel. It is evaluated at the initial configuration, where the dihedral angle is zero, and torque required from the magnet will be maximal. The mass given by (19) will also depend on the external magnetic field H direction. Choice of H is described in Section III-B.3.

2) Magnet Direction: Equation 19 gives the mass of the magnet when oriented such that the direction of magnetization is orthogonal to the hinge—i.e., the magnetic torque is not constrained by the hinge. However, as seen in Section II, such a magnet cannot always be fabricated. Therefore the planner must adjust the solution to use one of the three global directions described in Section II.

The planner initially chooses a set of magnet directions and runs the recursive algorithm using that set. It then rotates the set by a small increment and runs the recursive algorithm again. For each iteration, the planner finds the nearest global direction to the desired magnet direction—by projection of magnetic moment onto global magnet directions—and the magnet is scaled in that direction so that the component of torque parallel with the hinge axis from the scaled vector is equal to that of the original vector orthogonal to the hinge.

After incrementally rotating the set of magnet directions by 120° so that the full range of directions is tested, the global planner chooses the best solution. We define the best solution to be that which has the smallest maximum magnet size of all of the feasible solutions. Feasible solutions are those in which the magnet can geometrically fit on the face that it is actuating. Mass of the magnet is of course directly related to its volume, and area on the layout is found from the volume, given the electroplating thickness of the process.

3) External Field Direction: The magnet mass and direction are determined as in Sections III-B.1 and III-B.2 twice; once with positive H, and once with negative H. The larger of the two results is chosen. If a magnet of the determined size does not fit on the panel, given fabrication specifications, then the smaller magnet is determined. The field polarity used is recorded in association with that face.

The heuristic of choosing the direction requiring larger magnet mass tends to yield smaller magnets overall. If the direction that yields the smallest magnet is chosen in each step, long chains tend to have magnets of increasing size, pointing in the same direction. Eventually a magnet will need to face in another direction, and is used because magnets of larger mass can aid in rotation magnetic vectors of the children.

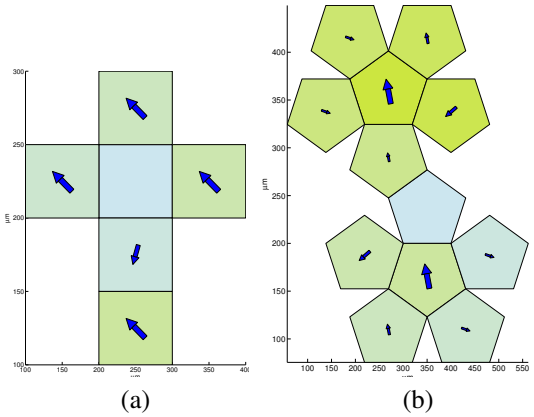

Fig. 6. Planar net and magnetic moments generated by planner on a (a) cube and (b) dodecahedron. Arrows represent μ (magnetization) vectors, and are scaled to approximate the area of the magnet on each face.

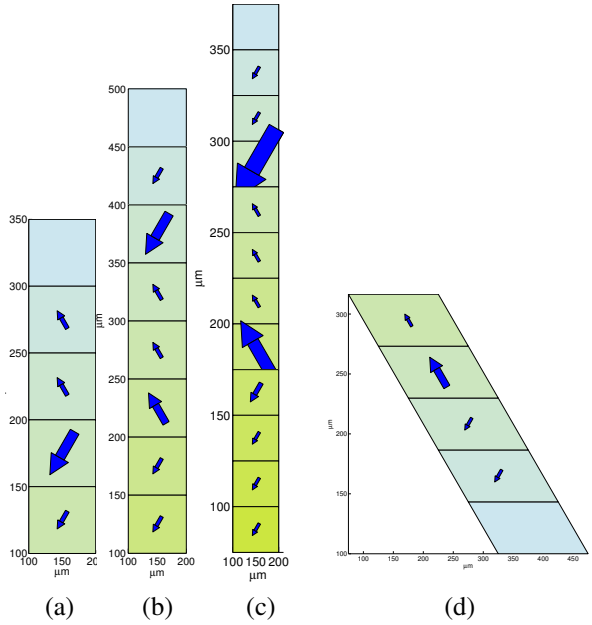

Fig. 7. Planar ne sequential chain of five panels (a), eight panels (b), and twelve panels (c). Arrows represent μ (magnetization) vectors, and are scaled to approximate the area of the magnet on each face. Also shown (d) are planar net and magnetic moments generated by planner on a sequential chain of five non-rectangular panels, forming a spiral. The sum of dihedral angles in each final assembly equals 360 degrees.

IV. EXPERIMENTAL AND SIMULATION RESULTS

A. Planner Results

We have run the planner on various shapes, as seen in Figures 6 and 7. In these figures, the arrows represent calculated μ (magnetization) vectors for magnets to be fabricated on each face. Arrows are scaled to indicate the area that would be required by a magnet of the strength determined by the planner, using magnets described below. The face with no arrow is the root face, and will be rigidly attached to the substrate. Face edges are 100μm long, and the mass of each face is approximately 0.04μg, based on a typical fabrication process using polysilicon as a structural material. Density of the cobalt platinum magnet is $11.5\frac{\text{g}}{\text{cm}^3}$. The external magnetic field strength is 250G, and magnetization per unit volume of the magnets was calculated to be $2.7 \times 10^{-2}\frac{\text{emu}}{\text{cm}^3}$, both based on the magnet described in Section IV-B. Magnet thickness is 180Å, and the minimum magnet mass is 1.9×10^{-9}g. The torque multiplier ϵ is -4.

B. Magnet Configuration Experiment

1) Experimental Setup: We electroplated, magnetized, and measured a prototype CoPt magnet in order to confirm the validity of a 120° magnet configuration. Specifically, we wish to show that magnets with fields offset by 120° can be magnetized on the same die, while allowing other magnets to retain a field.

Even though this preliminary process was not optimized to improve saturation or coercivity, the planner was able to find a solution when magnets such as this one are used. All planner results shown in this paper are based on the

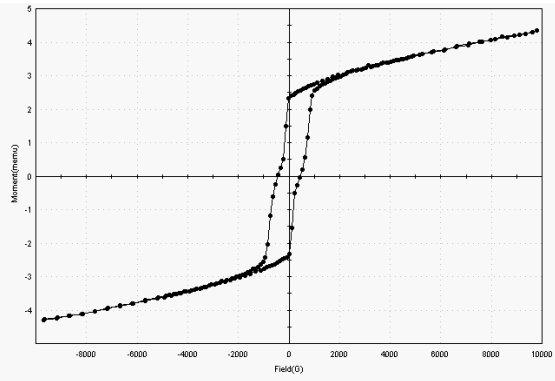

Fig. 8. Plot showing hysteresis of CoPt magnet. The magnet dimensions are $10mm \times 2mm$, and the hysteresis was measured along the long axis.

hysteresis characteristics of this magnet. The magnet is rectangular and measures 2mm by 10mm, and was deposited onto copper film which was sputtered onto a silicon wafer. The magnet was electroplated in a CoPt solution at $1.2v$, until an accumulated charge of 250mC was reached. The composition of the magnet was measured as approximately 79% cobalt and 21% platinum in an EDX SEM system. The hysteresis plot for the magnet measured along its long axis is shown in Figure 8.

2) Results: The magnet was first magnetized along its long (easy) axis in a field of 200G. The measured moment in this configuration was 2.2mEMU. The magnet was then rotated 120° and exposed to the same magnetizing field. This simulates magnetization of the second magnet orientation. The magnetic moment was measured again along its easy axis, and was found to be 1.7mEMU. The magnet was rotated another 120° and exposed to the magnetizing field for a third time. After this magnetization, the moment along the easy axis was measured as 1.63mEMU.

3) Discussion: This experiment shows that the magnet retains 77% of its original magnetization after exposure to the second field, and 74% after exposure to the third field. The hysteresis graph also shows that the coercivity is approximately $450G$ in the easy axis, while we applied a field of $200G$ offset from the easy axis. The small reduction in moment can be attributed to the component of the magnetizing field in parallel with the easy axis but opposite in direction, which is supported by the hysteresis data.

Based on this data, we conclude that it is possible to magnetize one magnet while not demagnetizing magnets in the two other orientations. Thus this configuration will enable batch magnetization of hard magnets in three different directions on a single die.

V. CONCLUSION

We have presented a new magnet configuration, and a corresponding algorithm for planning sequential assembly of complex microstructures. We demonstrated the feasibility of application of hard magnets in a 120° offset magnet configuration for batch fabrication and assembly of microstructures, using a macroscale test magnet. The planner was able to find solutions to various microstructures based on this magnet offset configuration. We believe that this is a promising foundation to the design and fabrication of self-assembled microstructures, which can eventually be used in to assembling microstructures of increasing complexity, broadening the application base of 3D microstructures.

A. Future Work

Microdevices designed using this method can be fabricated and assembled. These devices should be fabricated based on the layout and magnet sizes determined by the planner. Further automation of the design would have the planner generate the actual masks used for fabrication.

Theoretical results and additional improvements to the planner's application would also be of benefit. The planner would be more versatile with planning based on the dynamics of micropanels. We would also like to see what class of shapes can be handled by the planner. It may be possible to expand the class of shapes that the planner accepts to largely non-convex shapes, particularly in the layout and folding order.

ACKNOWLEDGMENTS

We would like to thank the Cornell NanoScale Science and Technology Facility (CNF) for teaching us about fabrication, and Alex Yan for help with magnetic materials processes and measurements at RPI.

REFERENCES

[1] S. Avadhanula and R. S. Fearing. Flexure design rules for carbon fiber microrobotic mechanisms. In *IEEE International Conference on Robotics and Automation*, pages 1579–1584, Barcelona, Spain, April 2005.

[2] F. Dinelli, S. K. Biswas, G. A. D. Briggs, and O. V. Kolosov. Ultrasound induced lubricity in microscopic contact. *Applied Physics Letters*, 71:1177–1179, September 1997.

[3] R. S. Fearing, K. H. Chiang, M. H. Dickinson, D. L. Pick, M. Sitti, and J. Yan. Wing transmission for a micromechanical flying insect. *IEEE International Conference on Robotics and Automation*, pages 1509–1516, April 2000.

[4] Ville Kaajakari and Amit Lal. Thermokinetic actuation for batch assembly of microscale hinged structures. *IEEE Journal of Microelectromechanical Systems*, 12(4):425–432, August 2003.

[5] Paul E. Kladitis and Victor M. Bright. Prototype microrobots for micro-positioning and micro-unmanned vehicles. *Sensors and Actuators A: Physical*, 80(2):132–137, 2000.

[6] E. J. J. Kruglick, B. A. Warneke, and K. S. J. Pister. CMOS 3-axis accelerometers with integrated amplifier. *The Eleventh Annual International Workshop on Microelectromechanical Systems Proceedings*, pages 631–636, January 1998.

[7] Liang Lu and Srinivas Akella. Folding cartons with fixtures: A motion planning approach. *IEEE Transactions on Robotics and Automation*, 16(4):346–356, August 2000.

[8] Ronald T. Merrill, Michael William McElhinny, and Phillip L. MacFadden. *The Magnetic Field of the Earth: Paleomagnetism, the Core, and the Deep Mantle*. Elsevier Science & Technology Books, 1998.

[9] J. O'Rourke. Folding and unfolding in computational geometry. In *Proc. Japan Conf. Discrete Comput. Geom. '98*, pages 142–147, December 1998.

[10] G. C. Shephard. Convex polytopes with convex nets. *Mathematical Proceedings of the Cambridge Philosophical Society*, 78:389–403, 1975.

[11] B. Wagner and W. Benecke. *Magnetically Driven Microactuator: Design Considerations*. Springer Verlag, 1990.

[12] Ming C. Wu. Micromachining for optical and optoelectronic systems. *Proceedings of the IEEE*, 85(11):1833–1856, November 1997.